

# Microstructure of Hydrogenated Magnesium–Nickel Eutectic Alloy Based Composites and its Changes during Hydrogen Absorption/Desorption Cycling

P. V. Fursikov<sup>a, \*</sup>, V. N. Fokin<sup>a</sup>, E. E. Fokina<sup>a</sup>, A. A. Arbuzov<sup>a</sup>, I. I. Khodos<sup>b</sup>,  
M. V. Lototskiy<sup>a, c</sup>, and B. P. Tarasov<sup>a</sup>

<sup>a</sup> Federal Research Center of Problems of Chemical Physics and Medicinal Chemistry, Russian Academy of Sciences, Chernogolovka, Moscow oblast, 142432 Russia

<sup>b</sup> Institute of Microelectronics Technology and High Purity Materials, Russian Academy of Sciences, Chernogolovka, Moscow oblast, 142432 Russia

<sup>c</sup> University of the Western Cape, HySA Systems Centre of Competence, X17, Belville, 7535 South Africa

\*e-mail: fpv@icp.ac.ru

Received July 10, 2023; revised July 10, 2023; accepted July 10, 2023

**Abstract**—In this work, we studied phase composition, hydrogen desorption kinetics and microstructural topology of hydrogen-sorbing composite materials prepared by ball milling under hydrogen of the powders of Mg<sub>89</sub>Ni<sub>11</sub> eutectic alloy without and with additive of graphene-like material (GLM). It was shown that in both cases the reproducible fast desorption kinetics were achieved after the fifth dehydrogenation—re-hydrogenation cycle. Using transmission electron microscopy, selected area electron diffraction, and the effect of MgH<sub>2</sub> radiolysis it was found that after seven hydrogenation—dehydrogenation cycles the material retains a highly dispersed microstructure: in the regions with a cross-sectional area of 1 micron in the size there are grains of Mg and Mg<sub>2</sub>Ni hydride-forming phases that are in direct contact, that favors the hydrogen sorption performance of the material.

**Keywords:** magnesium alloys, metal hydride, composite, microstructure, electron microscopy

**DOI:** 10.1134/S0018143923080106

## THEORETICAL ANALYSIS

Magnesium attracts much attention from researchers as a cheap and nature-friendly material for the reversible hydrogen storage due to the high hydrogen content in the hydride MgH<sub>2</sub> (7.6 wt %) [1–3]. However, the high enthalpy of formation of the MgH<sub>2</sub> phase (75 kJ/mole H<sub>2</sub>), the poor thermal conductivity of MgH<sub>2</sub>, and the low rate of hydrogen sorption—desorption in magnesium caused by the high energy barrier (about 1 eV) of dissociation of H<sub>2</sub> molecules on the metal surface and slow hydrogen diffusion in the MgH<sub>2</sub> phase prevent widespread use of individual magnesium for these purposes [4].

It has been known that a significant improvement in the hydrogen sorption properties of magnesium materials can be achieved by forming Mg-based powder composites, in which (1) the grain sizes of hydride-forming phases in the composite particles are in the submicro- and nanoscales [1], and (2) within which additives are introduced to catalyze the dissociation of hydrogen molecules on the surface of hydride-forming phases and simultaneously provide good heat transfer in powder composites [5]. Earlier, we reported another

promising way to prepare such a hydrogen storage material: a powder composite based on magnesium-nickel eutectic alloy (Mg+Mg<sub>2</sub>Ni) with a highly dispersed microstructure mixed with GLM additives [5].

The Ni-containing phases of various intermetallics, including LaNi<sub>5</sub> and Mg<sub>2</sub>Ni, have been widely reported [6–11] to accelerate the reaction between the Mg phase and hydrogen. This fact is due to that these intermetallic compounds, which have catalytic sites on the surface facilitating the dissociation of H<sub>2</sub> molecules, provide a possibility of transporting H atoms through the interface between the active phase of the intermetallic compound and the magnesium phase. Thus, the hydrogen sorption performances of composites based on Mg–Ni eutectic alloys depend on their microstructural characteristics, especially, the grain size of Mg and Mg<sub>2</sub>Ni phases and the mutual spatial arrangement of the phases in composite particles. The more efficient catalytic and H atoms transfer behavior of Mg<sub>2</sub>Ni is favored by the highly dispersed microstructure of the Mg–Ni eutectic alloy conditioning a large area of interphase boundaries between Mg and Mg<sub>2</sub>Ni.

A question of whether these topological features of the microstructure of powder composites based on Mg–Ni alloys are preserved during hydrogen absorption–desorption processes can be investigated by transmission electron microscopy (TEM) and selected area electron diffraction (SAED), since, as it mentioned above, the grain sizes of hydride-forming phases in composite particles lie in the submicro- and nanoscale. Thus, the purpose of our work was to study the mutual spatial arrangement of hydride-forming phases in hydrogenated powder composites based on the Mg–Ni eutectic alloy before and after hydrogen desorption–absorption cycles.

## EXPERIMENTAL

MgH<sub>2</sub> samples were prepared using Mg 200 μm-powder with a purity of 99.95 wt %. The starting components for preparing the Mg–Ni composites were an eutectic alloy of Mg (purity 99.95 wt %) with Ni (purity 99.99%) with the elemental composition Mg<sub>89</sub>Ni<sub>11</sub> (a detailed procedure for melting and characterizing the alloy was reported in [4]) and a carbon material with the graphene-like structure (GLM) with a specific surface area of 600–620 m<sup>2</sup>/g. The synthesis technique and physico-chemical characteristics of the GLM were described in detail in [1]. The alloy was preliminarily ground to chips in a glove box under argon atmosphere (water and oxygen content no more than 0.0001%) and mixed with GLM (the mass ratio was 9 : 1).

Hydrogen-containing powder samples of magnesium hydride and Mg–Ni alloy were fabricated by mechanochemical treatment in a Fritsch Pulverisette 6 planetary ball mill under hydrogen pressure in the grinding bowl of 30 atm. The grinding time was 10 h, rotation speed 400 rpm, the ball-to-sample mass ratio 50 : 1. High-purity hydrogen (99.999%) was used. The synthesized samples were subjected to 7 hydrogen desorption–absorption cycles carried out using a laboratory Sieverts setup. H absorption was carried out at 300°C and 10 atm H<sub>2</sub> for 30 min, desorption at 350°C and 1 atm H<sub>2</sub> for 30 min. After completing the desorption–absorption cycles, the reactor with the sample was cooled to room temperature for about 3 h under a hydrogen pressure in the system of 10 atm.

The phase composition of the materials was studied by XRD using a Thermo Scientific ARL X'TRA powder diffractometer at room temperature (CuKα radiation, 2θ = 20°–80°). Since powder X-ray diffraction patterns of Mg–Ni composites were characterized by a high background level, especially in the region of small diffraction angles, and a low signal-to-noise ratio, for the convenience of visual perception and detailed analysis of the X-ray diffraction patterns, their diffraction peaks were approximated by sets of the pseudo-Voigt functions with the corresponding background subtraction. The microstructure of the

samples was studied by transmission electron microscopy (TEM) and selected area electron diffraction (SAED) using a JEOL JEM-2100 electron microscope at accelerating voltage of 200 kV.

## RESULTS AND DISCUSSIONS

According to XRD data (Fig. 1) the powder samples of the hydrogenated Mg–Ni alloy mainly contain two crystalline phases: α-MgH<sub>2</sub> (the structural type of rutile; space group *P4<sub>2</sub>/mnm*, #136) and pseudo-high-temperature Mg<sub>2</sub>NiH<sub>4</sub> hydride with a disordered cubic structure (space group *Fm–3m*, #225). Some amount of Mg<sub>2</sub>NiH<sub>0.3</sub> phase (the saturated solid solution of hydrogen in the intermetallic compound; space group *P6<sub>2</sub>22*, #180) is also present due to incomplete hydrogenation of Mg<sub>2</sub>Ni caused by the fact that at the applied hydrogenation conditions (10 atm H<sub>2</sub>, 300°C), the hydrogen pressure was very close to the absorption plateau pressure in H<sub>2</sub>–Mg<sub>2</sub>Ni system [12].

It is seen from Fig. 1a that after the first hydrogenation by ball milling in H<sub>2</sub> the XRD pattern exhibits wide diffraction peaks and low signal-to-background ratio due to the nanocrystalline structure of the ball milled material [7]. After completion of seven dehydrogenation–re-hydrogenation cycles, the peaks become narrower and more intensive (Fig. 1b) that indicates an increase in the size of the coherent scattering domains (CSD) in the crystal lattice of the hydride phases during hydrogen desorption–absorption cycling. For example, Scherrer estimation of the line broadening for α-MgH<sub>2</sub> in the direction [110] shows increase of the CSD size from 12 ± 2 nm for the as-milled sample to 66 ± 8 nm for the cycled one.

Kinetic curves of hydrogen desorption are presented in Fig. 2. It is seen that even after the fifth desorption half-cycle, the ratio (*V/V<sub>0</sub>*) of the observed amount of desorbed H<sub>2</sub> to the theoretical one calculated assuming complete hydrogenation is significantly lower than 1, that indicates incomplete hydrogenation of the alloy under the experimental conditions. These data are consistent with the XRD results (Fig. 1), which demonstrate that the hydrogenated Mg–Ni alloy contains a noticeable amount of the Mg<sub>2</sub>NiH<sub>≤0.3</sub> phase. Also, the XRD data for these samples showing the absence of non-hydrogenated Mg phase are consistent with the fact that *V/V<sub>Mg</sub>* values are higher than 1 from the 4-th desorption cycle forth.

As we reported earlier [1], addition of graphene-like material (GLM) significantly accelerates dehydrogenation and re-hydrogenation of magnesium hydride prepared by reactive ball milling in H<sub>2</sub>, presumably, due to improvement of heat transfer in the sample powder by GLM. The kinetic improvements were insignificant in our case when the rates of H<sub>2</sub> desorption were very close for hydrogenated Mg–Ni with and without GLM additive. At the same time,

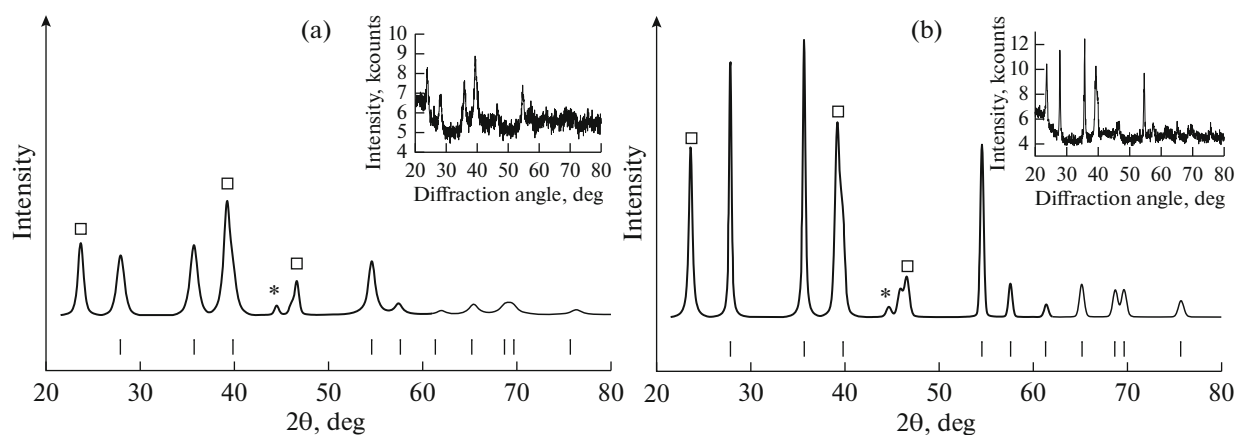


**Fig. 1.** Indexed XRD patterns (background subtracted) of the hydrogenated Mg–Ni eutectic alloy: (a) as milled; (b) after 7 dehydrogenation–re-hydrogenation cycles. The boxes and asterisks mark XRD peaks of  $\text{Mg}_2\text{NiH}_4$  and  $\text{Mg}_2\text{NiH}_{0.3}$  phases, respectively. Bottom ticks mark angular positions of Bragg reflections from  $\alpha\text{-MgH}_2$  with the relative theoretical intensities above 5. The intensities (Y-axes) are shown in arbitrary units (same for both patterns). The as-measured patterns are shown in the insets.

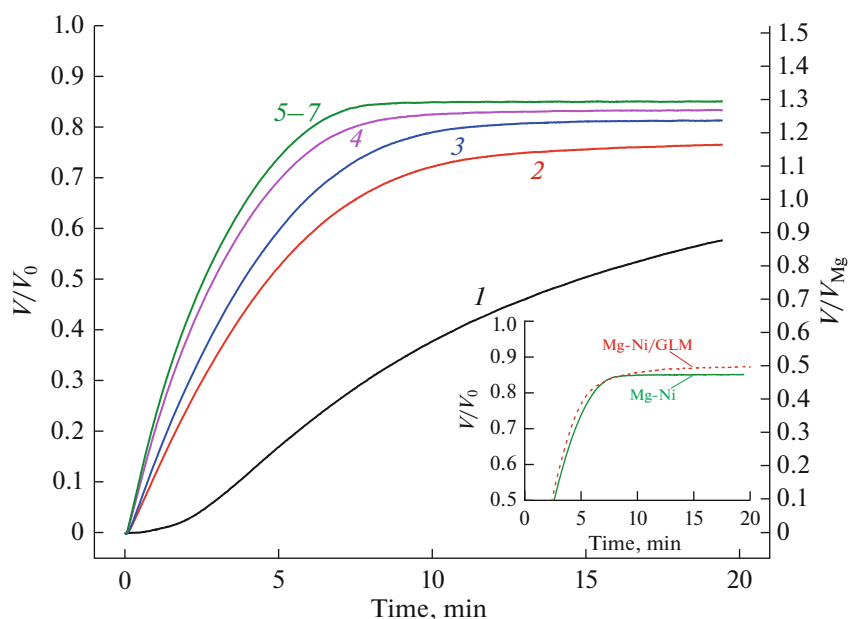


**Fig. 2.** Curves of the consecutive half-cycles of hydrogen desorption (the numbers are shown by curve labels) from the hydrogenated Mg–Ni eutectic alloy.  $V$ —the released moles of  $\text{H}_2$ , as measured;  $V_0$ ,  $V_{\text{Mg}}$ —the theoretical amounts of  $\text{H}_2$  (moles) that the respective amounts of  $\text{Mg} + \text{Mg}_2\text{Ni}$  and  $\text{Mg}$  in the alloy can absorb. The inset shows the curves for the 5<sup>th</sup> hydrogen desorption for the Mg–Ni alloy and its composite with GLM (9/1 mass ratio).

while in the latter case the dehydrogenation stopped at the conversion fraction  $V/V_0 = 0.85$ , at presence of GLM it continued to increase and achieved  $V/V_0 = 0.875$  after 20 min from desorption start (see inset in Fig. 2) thus confirming the role of GLM in the improvement of cycle stability of nanostructured Mg-based hydrides by prevention of sintering of their particles at high temperature [1, 5].

The phase of hydrogen solid solution in  $\text{Mg}_2\text{Ni}$  intermetallic ( $\text{Mg}_2\text{NiH}_{0.3}$ ) is known as an efficient cat-

alyst of hydrogenation of Mg and dehydrogenation of  $\text{MgH}_2$  [13, 14]. Also, as follows from the data reported in [15], at  $300^\circ\text{C}$   $\text{Mg}_2\text{NiH}_{0.3}$  exhibits thermal conductivity sufficiently higher than that for the hydride phase  $\text{Mg}_2\text{NiH}_4$ . Thus, we believe that during hydrogen absorption and desorption at the applied experimental conditions, H desorption kinetics and heat transfer in the Mg–Ni(H) powder are facilitated by the remaining amount of the  $\text{Mg}_2\text{NiH}_{0.3}$  which levels improvements of the  $\text{H}_2$  desorption rate caused by GLM additive in the Mg–Ni/GLM composite.

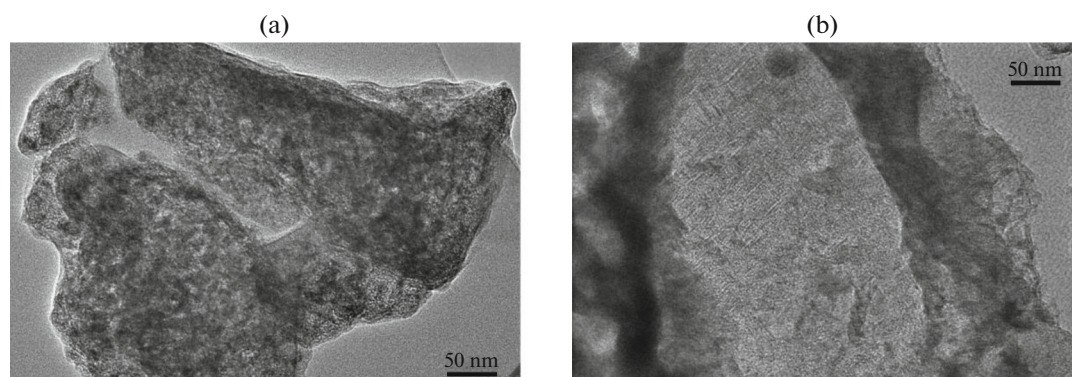


**Fig. 3.** TEM images (selected area) of single-phase  $\alpha$ - $\text{MgH}_2$  particles: (a) Image taken immediately after placing the specimen in the TEM chamber; (b) Image taken after 2 min exposure to the electron beam, which caused a clearly observed erosion of the magnesium hydride phase.

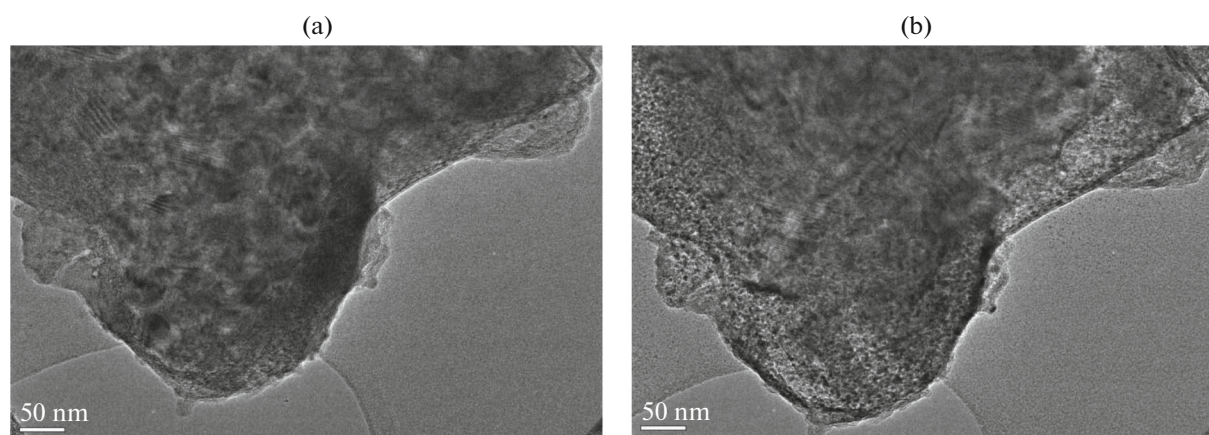


**Fig. 4.** TEM image and SAED pattern of the hydrogenated composite obtained after 2 min exposure to the electron beam.

The microstructure of the hydrogenated Mg–Ni alloy undergoes noticeable change after the first several cycles of hydrogen desorption–absorption, as evidenced by a comparison of the TEM (Figs. 3a, 3b) and XRD (Figs. 1a, 1b) data of the as-milled sample with those of the cycled one. The TEM images illustrate that the single-phase areas of the cycled alloy are larger than those for the as-milled one. The analysis results of the XRD patterns agree with the TEM data.

There are some difficulties occurring on studying the microstructure of hydrogenated magnesium alloys using TEM: for example, there is a problem of correct identification of regions of various types in a TEM image with phases that are present in the TEM specimen. The partial inelastic interaction of the electron beam with the specimen and a low partial hydrogen pressure in the TEM chamber result in a rather rapid loss of hydrogen by the magnesium hydride phase [16]. Due to presence of air traces in the TEM chamber the decomposition (radiolysis) of the  $\text{MgH}_2$  phase is also usually accompanied by the formation of the MgO phase in the specimen [17]. In order to retard the

decomposition process, TEM facilities with special low-temperature chambers and ultrahigh vacuum are used [17].

We have suggested a different way which avoids the mentioned complicated and expensive TEM equipment. Before the TEM and SAED studies of the heterophase Mg–Ni(H) material, we first took TEM and SAED calibration data for a powder of a single-phase  $\alpha$ - $\text{MgH}_2$ . In the course of the calibration observations, we used the reported [18] value of the so-called characteristic time (the time of 200 keV electron beam irradiation after which  $1/e = 37\%$  of the initial  $\alpha$ - $\text{MgH}_2$  is left in the specimen) as approximately 2 min. TEM micrographs obtained immediately after placing the  $\alpha$ - $\text{MgH}_2$  specimen in the TEM chamber and after 2 min of the electron beam irradiation are shown in Fig. 4.

TEM images of eroded  $\text{MgH}_2$  were used when studying the microstructure of the hydrogenated Mg–Ni eutectic alloy. The SAED data taken from an area of the specimen with a cross-sectional diameter of

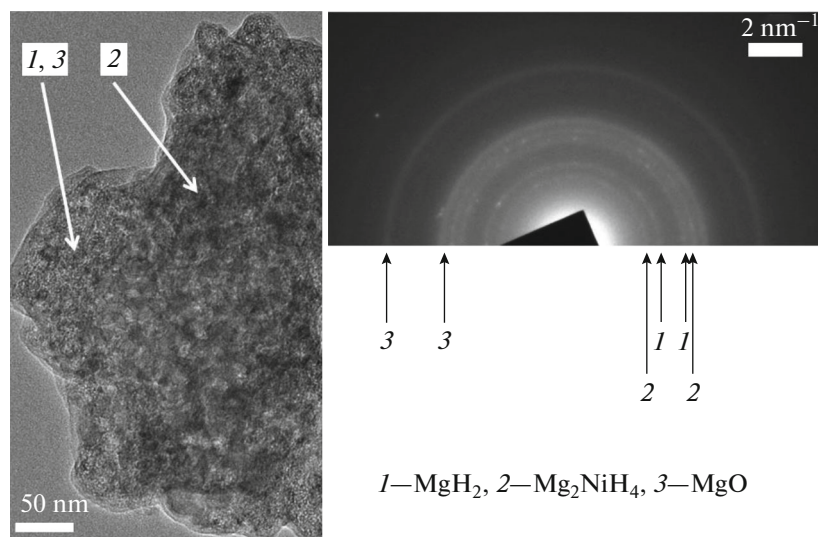


Fig. 5. TEM images (selected area) of the as-prepared (a) and cycled (b) hydrogenated Mg–Ni eutectic alloy.

~1 micron (Fig. 4) indicate the  $\alpha$ -MgH<sub>2</sub> and Mg<sub>2</sub>NiH<sub>4</sub> phases are located in common within the area. Due to the small size and low crystallinity of the phases formed during the erosion of the specimen and their products of interaction with residual gases in the TEM chamber, the corresponding diffraction rings will be diffuse, that does not allow clear distinguishing these phases in the SAED patterns. An exception is the MgO phase (fcc structure): the first two main diffraction rings corresponding to it are clearly distinguishable in the SAED pattern (Fig. 5). In TEM images of the hydrogenated composite (Fig. 5) there are visually distinguishable areas of two types, one of which corresponds to the magnesium hydride and magnesium oxide phases, and the other one corresponds to the Mg<sub>2</sub>NiH<sub>4</sub> phase. It can also be seen that these two areas are in direct contact that indicates the common interface between the Mg/MgH<sub>2</sub> and Mg<sub>2</sub>Ni/Mg<sub>2</sub>NiH<sub>≤0.3</sub>/Mg<sub>2</sub>NiH<sub>4</sub> phases.

## CONCLUSIONS

The catalyzed H atoms transfer and heat-conducting abilities of the Mg<sub>2</sub>Ni constituent of Mg–Ni alloy-based composites will be in common more favorable for enhancing hydrogen sorption and desorption rate if the intermetallic and magnesium phases in the composites have the interphase boundary area remaining large during hydrogen absorption-desorption cycles. The radiolysis of MgH<sub>2</sub> phase can be used in studying the microstructural topology of Mg–Ni alloy-based powder composites, in which the grains of the constituent phases are less than 1 micron in size. In doing so, the TEM electron beam serves as an etchant to achieve phase contrast in TEM images of the heterophase composites. For the correct interpretation of such

images, it is proposed to preliminary conduct a reference series of TEM and SAED observations of the single-phase samples corresponding to the hydrogenated constituents of the heterophase composite.

## FUNDING

This work was funded by the Ministry of Science and Higher Education of the Russian Federation (Megagrant, agreement number 075-15-2022-1126).

## CONFLICT OF INTEREST

The authors of this work declare that they have no conflicts of interest.

## REFERENCES

1. Tarasov, B.P., Arbuzov, A.A., Mozhzhuhin, S.A., et al., *Int. J. Hydrogen Energy*, 2019, vol. 44, p. 29212.
2. Baran, A. and Polański, M., *Materials*, 2020, vol. 13, p. 3993.
3. Ouyang, L., Liu, F., Wang, H., et al., *J. Alloys Compd.*, 2020, vol. 832, p. 154865.
4. Fursikov, P.V. and Tarasov, B.P., *Russ. Chem. Bull.*, 2018, vol. 67, p. 193.
5. Tarasov, B.P., Arbuzov, A.A., Volodin, A.A., et al., *J. Alloys Compd.*, 2022, vol. 896, p. 162881.
6. Fursikov, P.V., Borisov, D.N., and Tarasov, B.P., *Russ. Chem. Bull.*, 2011, vol. 60, p. 1848.
7. Yartys, V.A., Lototsky, M.V., Akiba, E., et al., *Int. J. Hydrogen Energy*, 2019, vol. 44, p. 7809.
8. Sun, Y., Shen, Ch., Lai, Q., et al., *Energy Storage Mater.*, 2018, vol. 10, p. 168.
9. Anbarasu, S., Muthukumar, P., and Mishra, S.C., *Heat Transfer Eng.*, 2014, vol. 35, p. 1354.

10. Tran, X.Q., McDonald, S.D., Gu, Q.F., and Nogita, K., *J. Alloys Compd.*, 2015, vol. 636, p. 249.
11. Grigorova, E., Tzvetkov, P., Todorova, S., et al., *Materials*, 2021, vol. 14, p. 1936.
12. Schefer, J., Fischer, P., Hälgl, W., et al., *J. Less-Common Met.*, 1980, vol. 74, p. 65.
13. Mazzaro, R. and Pasquini, L., *J. Alloys Compd.*, 2022, vol. 911, p. 165014.
14. Panda, S., Satya Aditya, M.V.V., Kutiyar, S., and Tati-parti, S.S.V., *Appl. Nanosci.*, 2023, vol. 13, p. 5755.
15. Blomqvist, H. and Noréus, D., *J. Appl. Phys.*, 2022, vol. 91, p. 5141.
16. Paik, B., Jones, I.P., Walton, A., et al., *Philos. Mag. Lett.*, 2010, vol. 90, p. 1.
17. Danaie, M. and Mitlin, D., *J. Alloys Compd.*, 2009, vol. 476, p. 590.
18. Surrey, A., Schultz, L., and Rellinghaus, B., *Adv. Struct. Chem. Imaging*, 2016, vol. 2, p. 7.

**Publisher's Note.** Pleiades Publishing remains neutral with regard to jurisdictional claims in published maps and institutional affiliations.